Letter

Injection and confinement of positron bunches in a magnetic dipole trap

A. Deller [1,2,*] J. von der Linden [1,†] S. Nißl [1] K. Michishio [3] N. Oshima [3] H. Higaki [4] and E. V. Stenson [1]

[1] *Max-Planck-Institute für Plasmaphysik, 85748 Garching, Germany*

[2] *Physics Department, University of California, San Diego, La Jolla, California 92093, USA*

[3] *National Institute of Advanced Industrial Science and Technology (AIST), Tsukuba, Ibaraki 305-8568, Japan*

[4] *Graduate School of Advanced Science and Engineering, Hiroshima University, Hiroshima 739-8530, Japan*

(Received 25 April 2024; accepted 3 July 2024; published 9 August 2024)

We demonstrate the efficient injection of a pulsed positron beam into a magnetic dipole trap and investigate the ensuing particle dynamics in the inhomogeneous electric and magnetic fields. Bunches of $\sim 10^5$ e^+ were transferred from a buffer-gas trap into the field of a permanent magnet using a lossless E×B drift technique. The $\Delta t \approx 0.2$ μs pulses were short compared to the toroidal rotation period, $\tau_d \approx 16$ μs, and e^+ confinement time, $\tau_c \approx 0.6$ s. The redistribution dynamics were studied by measuring the delayed γ-ray emission as the trap was emptied. This work extends the record for the number of low-energy positrons held in a dipole trap by two orders of magnitude and represents a significant advance toward the confinement of an electron-positron pair plasma.

DOI: 10.1103/PhysRevE.110.L023201

Dipole magnetic fields generated by planetary and stellar dynamos commonly trap magnetized plasma [1]. Charged particles with a sufficiently large pitch angle (between the velocity vector, **v**, and the magnetic field, **B**) magnetically mirror between the high-field regions at the poles. The field gradient and curvature cause the poloidally bouncing particles to drift azimuthally on toroidal surfaces [2]. Collisions can scatter the particles across field lines or into the "loss cone" [3,4], or nonaxisymmetric field perturbations or plasma instabilities can drive radial diffusion and plasma flows [5–7]. Although the gyro, bounce, and drift motions of charged particles in dipole magnetic fields are well understood, the ubiquity and importance of astrophysical dipoles [8–12] and the special forms of plasma waves and particle transport they support [13–18] have motivated numerous efforts to study dipole traps in the laboratory [19–26].

A permanent magnet supported in vacuum is arguably the simplest implementation of a dipole trap. In the low-density regime, confinement of magnetized charged particles is typically limited by pitch-angle scattering [22]. However, the trapping time can be extended for a single charge species by biasing the magnet to plug the loss cone [27]. Alternatively, a levitating superconducting coil can be used to generate the dipole field [28]. In contrast to a permanent magnet, a floating coil possesses closed field lines that pass uninterrupted through its interior—i.e., mirroring and passing orbits are possible and neutral or single-component plasmas can be confined for times that exceed the collision time [29–33]. Levitating dipole traps require no plasma current and can be built on the cm scale [34,35], which makes them suitable for confining low-temperature electron-positron pair plasmas [36]. Pair plasmas likely occur in extreme astrophysical environments [37–40] and fundamentally differ from ion-electron plasmas because of their perfect mass symmetry [41]. Experimental pair plasma research has progressed considerably in recent years [42–49], and magnetically trapped electron-positron plasmas are expected to exhibit remarkable stability [50]. However, to test this prediction, new techniques are needed to combine low-energy electrons and positrons at plasma densities.

In this Letter, we demonstrate lossless drift injection [51] of bunches of e^+ into a supported magnetic dipole trap. Time-resolved measurements of the annihilation radiation were used to efficiently optimize the injection scheme and to study the toroidal expansion of the bunches as they drifted around the permanent magnet. Ultimately, we aim to employ these new techniques to produce a neutral pair plasma by mixing low-energy positrons and electrons in a levitating dipole trap [36].

Positrons from a linear-accelerator-based slow positron beam [52] were accumulated in a buffer-gas trap (BGT) [53–55], compressed to a diameter of ∼2 mm [56–58], and cooled via inelastic collisions with N_2 and CF_4 [59,60]. Every 3 s, approximately $N \approx 8\times10^4$ e^+ were ejected from the BGT in a $\Delta t = 180$ ns full-width-half-max (FWHM) pulse with a mean parallel energy of $\langle K_\parallel \rangle = 6.2$ eV and a FWHM spread of $\Delta K_\parallel = 0.8$ eV [61]. The bunches were magnetically guided through a pumping restriction and a downward-curving solenoid, and into the trap chamber—see Fig. 1(a). Two pairs of steering coils were used to adjust the position of the beam within the bend. A 250 mm diameter "boost coil" connected the transport magnetic field lines with the open field lines leading to the permanent magnet.

*Contact author: adam.deller@ipp.mpg.de

†Contact author: jens.von.der.linden@ipp.mpg.de

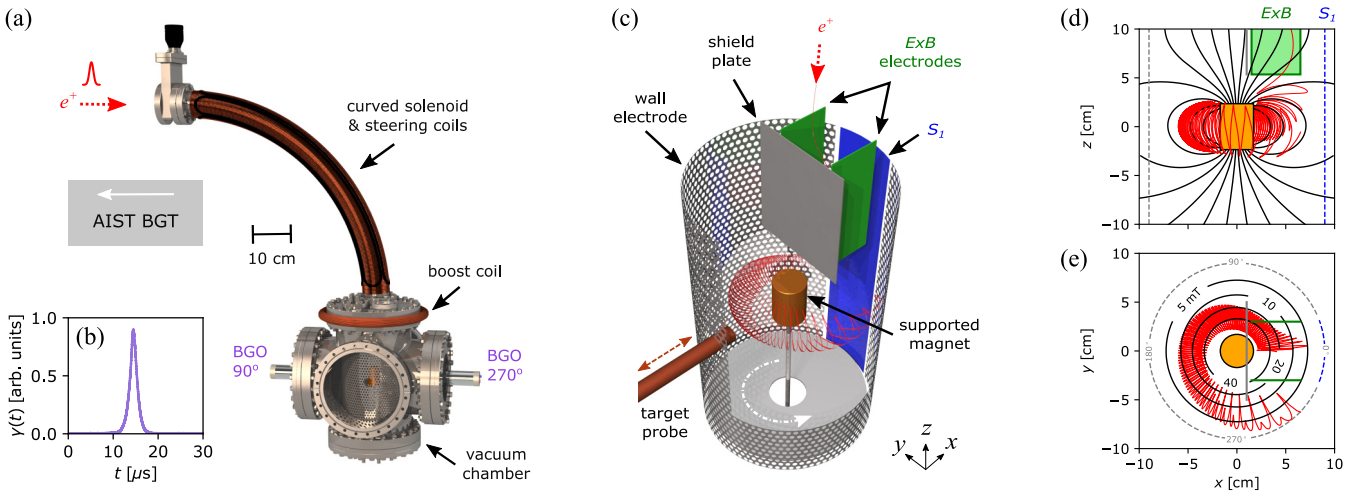

FIG. 1. (a) Dipole trap and γ-ray detectors; the target probe mounts to the nearside flange that has been omitted from the illustration to reveal the trap location. (b) Example of the delayed annihilation signal that signifies successful injection. (c) Supported magnet (orange), E×B (green), S_1 (blue), and wall electrodes (partial cutaway view), shield plate, and retractable target probe. The red path represents a calculated trajectory for a 6 eV positron in static injection fields; the white curved arrow (dash dot) shows the drift direction. The trajectory is projected onto the xz and xy planes in (d) and (e), respectively. (d) Dipole magnetic field lines ($y = 0$). (e) Contours of magnetic field strength [mT] in the midplane of the magnet ($z = 0$).

The magnetic dipole trap is depicted in Fig. 1(c). The confinement volume extends from the surface of the 33 mm diameter and 46 mm tall cylindrical magnet case to the 180 mm diameter wall electrode. The perforated stainless steel wall electrode is segmented into two unequal sectors. Cartesian (x, y, z) and cylindrical (r, θ, z) coordinates are used to denote positions in and around the dipole trap; the origin is defined as the center of the permanent magnet, which is supported in the vacuum chamber with its poles aligned vertically ($\hat{z}$). The magnetic field strength is ∼430 mT at the top of the magnet case and ∼3 mT in the midplane at the surface of the wall electrode ($r = 90$ mm, $z = 0$). The magnetic field lines in the xz plane are shown in Fig. 1(d) and the field strength in the xy plane is plotted in Fig. 1(e).

A lossless drift-injection technique was employed to push the positron bunches across the transport field lines and into the dipole field surrounding the permanent magnet [51]. A typical injection trajectory is shown in Figs. 1(c)–1(e). The red line represents the calculated path taken by a 6 eV positron in the combined electric and magnetic fields of the trap [62]. The particle enters the chamber at $\theta = 0°$ with a radial offset of $r = 50$ mm ($x = 50$ mm, $y = 0$) and passes between a pair of 118 mm long steel electrodes located at $y = \pm 30$ mm. The parallel plates are biased to $U_{\mathrm{E\times B}} = \pm 217$ V to generate an electric field of $\mathbf{E} \approx 65\,\hat{y}$ V/cm. The 1/8th sector electrode (S_1) is biased to +20 V and the magnet case is biased to $U_m = +14$ V. The electric field between the E×B plates, the magnet case, S_1, and the grounded wall electrode, superimposed with the magnetic field, results in a succession of bounces and drifts that maneuver the particle into the trap. The nonuniform magnetic field and radial electric field cause the particle to drift around the magnet in the anticlockwise direction (viewed from above) with an overall drift velocity,

$$\mathbf{v}_d = \mathbf{v}_R + \mathbf{v}_{\nabla B} + \frac{\mathbf{E}\times\mathbf{B}}{|\mathbf{B}|^2}, \tag{1}$$

where $\mathbf{v}_R$ and $\mathbf{v}_{\nabla B}$ are the magnetic curvature and gradient drift velocities [63]. After orbiting approximately 120° around the permanent magnet, the particle is shielded from the injection electric field and the radial position stabilizes at $r \sim 5$ cm. At $\theta = 240°$, the trajectory is once again affected by the injection electric fields, which push it outwards and into the wall.

Drift injection can be 100% efficient, provided the positron beam has a narrow energy spread, small diameter, and enters the drift region near the $y = 0$ plane [51]. The injection parameters were initially selected based on the results of previous experiments and simulations [62], and then iteratively tuned by scanning the currents supplied to the steering coils and boost coil, and the voltages applied to the E×B and S_1 electrodes. When the positrons were injected successfully, the annihilation of the bunch was delayed by one toroidal rotation period ($\tau_d \sim 16$ μs)—see Fig. 1(b). The annihilation time was measured using a similar technique to single-shot positron annihilation lifetime spectroscopy (SSPALS) [64], which was originally developed to study positronium [65].

Annihilation γ-rays were detected by three Bismuth Germanate (BGO) scintillators (decay time ∼1 μs [66]) coupled to photomultiplier tubes. The detectors were mounted inside re-entrant vacuum ports at $\theta = 0°$, 90°, and 270°, with the BGO crystals located near $r = 12$ cm. The detectors were adjusted for low gain to ensure that the output would not be saturated by the γ-ray burst produced by the injected bunch of positrons hitting the wall. Figure 2(a) shows a collection of time-resolved annihilation lifetime spectra measured using the 270° detector. Data obtained for a range of electric fields applied between the E×B electrodes are stacked along the horizontal axis. The BGT ejection time defines $t = 0$. When the applied voltages were smaller than $U_{\mathrm{E\times B}} = \pm 120$ V, the signal peaked at $t = 2$ μs, indicating prompt annihilation and failed injection. For larger voltages, the positrons were successfully injected and subsequently drifted around the magnet until they hit the target probe [the 15 mm diameter, retractable

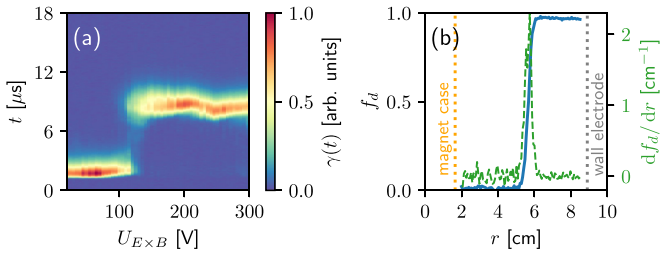

FIG. 2. (a) Time-dependent annihilation signal during e^+ injection for a range of voltages applied to the E×B electrodes. The target probe was fully inserted. (b) The fraction of γ-rays detected after $t = 12$ μs for different target probe positions (solid line; left axis) and the delayed signal differentiated by the probe position (dashed line; right axis). $U_m = +8$ V.

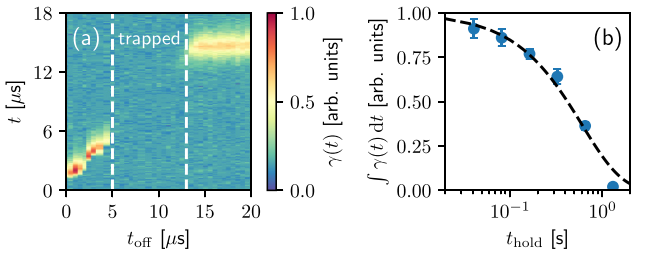

FIG. 3. (a) Time-dependent annihilation signal observed as the switch-off time of the injection voltages was varied. $U_m = +8$ V. (b) Mean (points) and standard deviation (bars) of the total γ-ray signal from all detectors observed at the end of a given hold time and an exponential fit (dashed line) to the data. $U_m = +14$ V.

copper rod shown in Fig. 1(c)] at $t \sim 9$ μs. The detector had a similar solid-angle view of the injection and probe positions ($\theta = 0°$ and 180°), and the signal amplitude was roughly equal for successful and failed injection. For the standard injection voltages, no prompt signal was observed because all of the positrons annihilated at the probe.

The radial distribution of the injected bunch was measured by moving the target probe horizontally through the trapping volume. With the target probe fully retracted, the positrons were able to complete an almost full orbit of the trap, and the peak in the annihilation signal shifted from $t \sim 9$ μs to 15 μs. Figure 2(b) shows the delayed fraction [64],

$$f_d = \frac{\int_B^C \gamma(t)\,\mathrm{d}t}{\int_A^D \gamma(t)\,\mathrm{d}t}, \tag{2}$$

($A = 0$, $B = 12$ μs, $C = 17$ μs, and $D = 20$ μs) that was measured with the 270° BGO as the probe was re-inserted stepwise into the trap. Differentiating f_d by the position of the tip of the target probe indicates that the injected positron bunch had an approximately Gaussian midplane radial distribution with a mean value of $r = 57$ mm and a FWHM of $\Delta r = 4.4$ mm.

To confine positrons for multiple toroidal periods, the injection electric field must be removed before it drives the antiparticles into the wall [27]. Additional injection measurements were conducted with the biases applied to the E×B and S_1 electrodes switched to ground after injection. Figure 3(a) shows the γ-ray signal recorded by the 0° BGO as the switching delay, t_{off}, was varied. When the biases were grounded too early ($t_{\mathrm{off}} < 5$ μs), the positron bunches were not injected successfully and the annihilation signal exhibited a prompt peak close to the switching time. Conversely, when the biases were switched off too late ($t_{\mathrm{off}} > 13$ μs), the positrons annihilated at $t \sim 15$ μs after one toroidal orbit of the trap. Between $t_{\mathrm{off}} = 5$ to 13 μs, the injection biases switched to ground whilst the positrons were safely within the $x < 0$ half of the trap. In this window, the annihilation signal is absent, which indicates that the injected positrons were captured with negligible losses.

Figure 3(b) shows the total annihilation signal from all three BGO detectors integrated over a 30 μs time window during which captured positrons were ejected from the trap by switching the magnet bias off and the injection electrodes back on. The hold time prior to ejection was varied within the range $t_{\mathrm{hold}} = 40$ ms to 1.3 s. An exponential fit to the data suggests that the mean lifetime of positrons in the trap was $\tau_c = 610 \pm 81$ ms. The pressure in the vacuum system was roughly $\sim 10^{-6}$ Pa. Previous work concluded that the e^+ confinement time is probably limited by outward diffusion driven by collisions with background neutrals [27].

Immediately after injection, the positron bunches occupied ~10% of the torus. To investigate the evolution of the azimuthal distribution, trap-and-hold measurements were made using hold times similar to the toroidal drift period ($\tau_d \approx 16$ μs). Figures 4(a) and 4(b) show the γ-ray signal (summed from all three BGO detectors) that was observed after ejecting the trapped positrons by reintroducing the injection electric field. For these measurements, the magnet case was statically biased to either $U_m = 14$ V or 30 V. The phase of the toroidal orbits determines the lag between the application of the electric field and the positrons being pushed into the wall, which resulted in clear diagonal striations in the annihilation data. The angular frequency of the drift motion was measured from

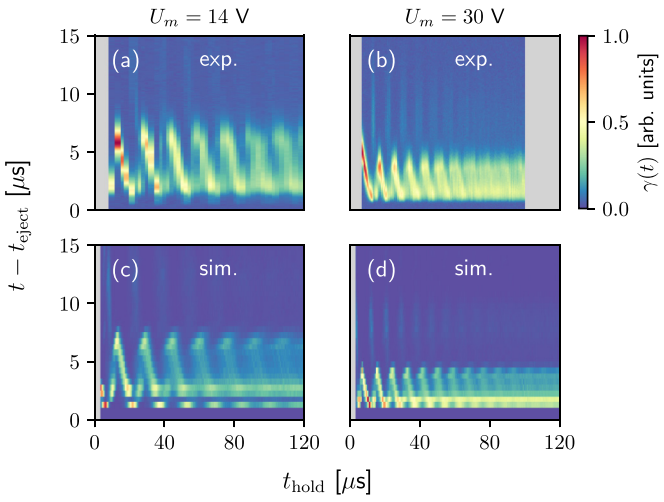

FIG. 4. (a), (b) Measured (sum of all three BGO detector data sets) and (c), (d) simulated annihilation signal for a range of short hold times in the dipole trap with the magnet case biased to either (a), (c) $U_m = +14$ V or (b), (d) +30 V.

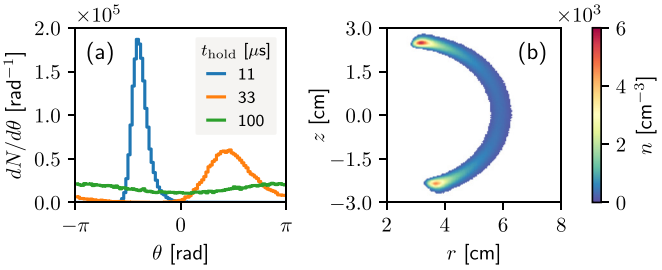

FIG. 5. Simulated (a) toroidal and (b) poloidal distribution of $N = 10^5$ e^+ in the dipole trap with $U_m = +14$ V. The color range in (b) has been clipped to show 90% of the distribution, which occupies a volume of ∼160 cm^3.

Fourier transforms of the stacked spectra to be $\omega_d = 405 \pm 2$ krad/s for $U_m = +14$ V, and $\omega_d = 734 \pm 4$ krad/s for $U_m = +30$ V. As expected, increasing the radial electric field resulted in a faster toroidal drift [Eq. (1)]. Toroidal expansion is evidenced by the diminishing contrast of the striations during the first 100 μs of confinement. The spatial profile and energy distribution of the injected beam determines the spread of drift frequencies that cause the initially clustered positrons to expand around the trap.

The experimental results are supported by simulations. Injection trajectories were calculated for 5000 positrons sampled from a model of the BGT distribution [54,62]. Figures 4(c) and 4(d) show sets of histograms of the times that the trajectories intersected a hard surface, which closely reproduce the main features of the annihilation data. Similar calculations were used to estimate the time-dependent toroidal distribution of $N = 10^5$ e^+ orbiting around the magnet [Fig. 5(a)], in addition to the post-expansion poloidal density distribution [Fig. 5(b)]. The simulations verify that the observed drift dynamics can be ascribed to single-particle behavior and allow us to determine the expectation value of the density of the expanded distribution, $\langle n \rangle \approx 10^3$ cm^{-3}. The magnetic field strength of the dipole decays with $1/r^3$ and the positron drift dynamics are, therefore, quite sensitive to the shape and position of the injected bunch. Consequently, measurements and simulations similar to those presented in Fig. 4 could be utilized to determine radial profiles without the need for target probe scans.

In conclusion, we have demonstrated lossless drift injection of a pulsed positron beam into a supported dipole trap. Approximately 10^5 e^+ were simultaneously confined by recapturing individual bunches produced by a BGT. This is at least two orders of magnitude more than has been achieved previously [27]. Time-resolved measurements of the annihilation radiation were used to distinguish between successful and failed injection of the pulsed beam, to efficiently optimize the capture scheme, and to observe the toroidal redistribution of the positrons during the initial stages of confinement. Trajectory calculations confirm that the observed dynamics are consistent with single-particle behavior.

A single-component collection of charged particles with a density, n, and temperature, T, is generally considered to be a non-neutral plasma if the Debye length, $\lambda_D = \sqrt{\epsilon_0 k_B T / n q^2}$, is small compared to the size of the distribution [67,68] (where q is the unit charge, ϵ_0 is the vacuum permittivity, and k_B is the Boltzmann constant). Inside the BGT, $\lambda_D \sim 2$ mm and the trapped positron clouds marginally qualify as plasma. However, after expanding toroidally in the dipole trap, the density was too low for collective effects to manifest. To obtain a non-neutral plasma would likely require $\gtrsim 10^7$ e^+ (which could be achieved by stacking bunches in a Penning trap [69–72]). In this case, the space-charge potential would be a sizable fraction of the electric potential applied to the magnet case. Accordingly, the techniques for measuring the toroidal drift frequency that we have described could be used to estimate the number of positrons in the plasma [73–75]. Our results are directly applicable to ongoing efforts to inject positron bunches into an electron plasma [76]. This work demonstrates the viability of drift injection with a bunched positron beam and represents an important step toward the confinement of a low-energy electron-positron pair plasma in a levitating dipole trap [36].

The authors are grateful to the APEX collaboration for supporting this work. We thank T. Hori for operating the LINAC, C. Hugenschmidt for providing the curved solenoid, and M. Singer for earlier development of the dipole trap. We are also very grateful to H. Saitoh for contributing to preparatory work and for many helpful discussions. Financial support was provided by the University of California San Diego Foundation, the European Research Council (741322), the Deutsche Forschungsgemeinschaft (HU 978/20-1, STE 2614/2-1), the Helmholtz Association (VH-NG-1430), and the Japanese Society for the Promotion of Science (KAKENHI 22H00115 and 22H04936). J.v.d.L. acknowledges support from the Alexander von Humboldt Foundation.

[1] F. Rincon, J. Plasma Phys. **85**, 205850401 (2019).
[2] T. G. Northrop and E. Teller, Phys. Rev. **117**, 215 (1960).
[3] V. V. Markellos, S. Klimopoulos, and A. A. Halioulias, Celest. Mech. **17**, 215 (1978).
[4] P. Porazik, J. R. Johnson, I. Kaganovich, and E. Sanchez, Geophys. Res. Lett. **41**, 8107 (2014).
[5] C. F. Kennel and H. E. Petschek, J. Geophys. Res. **71**, 1 (1966).
[6] A. W. Yau, T. Abe, and W. K. Peterson, J. Atmos. Sol. Terr. Phys. **69**, 1936 (2007).
[7] J. Pétri, Astron. Astrophys. **464**, 135 (2007).
[8] C. Størmer, Terr. Magn. Atmos. Electr. **35**, 193 (1930).
[9] N. Weiss, Astron. Geophys. **43**, 3.9 (2002).
[10] J. Pétri, J. Heyvaerts, and S. Bonazzola, Astron. Astrophys. **384**, 414 (2002).
[11] H.-B. Li, A. Goodman, T. K. Sridharan, M. Houde, Z.-Y. Li, G. Novak, and K. S. Tang, *Protostars and Planets VI*, edited by H. Beuther, R. S. Klessen, C. P. Dullemond, and T. Henning (University of Arizona Press, Tucson, 2014), pp. 101–124.
[12] V. M. Kaspi and A. M. Beloborodov, Annu. Rev. Astron. Astrophys. **55**, 261 (2017).
[13] B. Cerutti and A. M. Beloborodov, Space Sci. Rev. **207**, 111 (2017).

[14] B. M. Walsh and Y. Zou, J. Atmos. Sol. Terr. Phys. **219**, 105644 (2021).

[15] M. Ozaki, S. Yagitani, Y. Kasaba, Y. Kasahara, S. Matsuda, Y. Omura, M. Hikishima, F. Sahraoui, L. Mirioni, G. Chanteur, S. Kurita, S. Nakazawa, and G. Murakami, Nat. Astron. **7**, 1309 (2023).

[16] A. C. Boxer, R. Bergmann, J. L. Ellsworth, D. T. Garnier, J. Kesner, M. E. Mauel, and P. Woskov, Nat. Phys. **6**, 207 (2010).

[17] O. Adriani, G. C. Barbarino, G. A. Bazilevskaya, R. Bellotti, M. Boezio, E. A. Bogomolov, M. Bongi, V. Bonvicini, S. Borisov, S. Bottai, A. Bruno, F. Cafagna, D. Campana, R. Carbone, P. Carlson, M. Casolino, G. Castellini, L. Consiglio, M. P. D. Pascale, C. D. Santis *et al.*, Astrophys. J. Lett. **737**, L29 (2011).

[18] H. Saitoh, Z. Yoshida, Y. Yano, M. Nishiura, Y. Kawazura, J. Horn-Stanja, and T. S. Pedersen, Phys. Rev. E **94**, 043203 (2016).

[19] P. J. Baum and A. Bratenahl, Geophys. Res. Lett. **9**, 435 (1982).

[20] G. Yur, H. U. Rahman, J. Birn, F. J. Wessel, and S. Minami, J. Geophys. Res. **100**, 23727 (1995).

[21] J. C. Reardon, A. F. Almagri, N. Christensen, D. A. Endrizzi, C. B. Forest, S. Gallogly, A. Lambert, S. Malewicz, J. Milhone, P. D. Nonn, M. D. Nornberg, S. P. Oliva, and C. Purcell, Amer. J. Phys. **88**, 670 (2020).

[22] H. Saitoh, J. Stanja, E. V. Stenson, U. Hergenhahn, H. Niemann, T. S. Pedersen, M. R. Stoneking, C. Piochacz, and C. Hugenschmidt, New J. Phys. **17**, 103038 (2015).

[23] L. Gargaté, R. Bingham, R. A. Fonseca, R. Bamford, A. Thornton, K. Gibson, J. Bradford, and L. O. Silva, Plasma Phys. Control. Fusion **50**, 074017 (2008).

[24] B. A. Grierson, M. E. Mauel, M. W. Worstell, and M. Klassen, Phys. Rev. Lett. **105**, 205004 (2010).

[25] D. B. Schaeffer, F. D. Cruz, R. S. Dorst, F. Cruz, P. V. Heuer, C. G. Constantin, P. Pribyl, C. Niemann, L. O. Silva, and A. Bhattacharjee, Phys. Plasmas **29**, 042901 (2022).

[26] S. Bhattacharjee, A. R. Baitha, A. Nanda, S. Hunjan, and S. Bhattacharjee, Rev. Mod. Plasma Phys. **6**, 16 (2022).

[27] J. Horn-Stanja, S. Nißl, U. Hergenhahn, T. Sunn Pedersen, H. Saitoh, E. V. Stenson, M. Dickmann, C. Hugenschmidt, M. Singer, M. R. Stoneking, and J. R. Danielson, Phys. Rev. Lett. **121**, 235003 (2018).

[28] A. Hasegawa, L. Chen, and M. E. Mauel, Nucl. Fusion **30**, 2405 (1990).

[29] J. Kesner and M. Mauel, Plasma Phys. Rep. **23**, 742 (1997).

[30] Z. Yoshida, H. Saitoh, J. Morikawa, Y. Yano, S. Watanabe, and Y. Ogawa, Phys. Rev. Lett. **104**, 235004 (2010).

[31] H. Saitoh, Z. Yoshida, J. Morikawa, Y. Yano, T. Mizushima, Y. Ogawa, M. Furukawa, Y. Kawai, K. Harima, Y. Kawazura, Y. Kaneko, K. Tadachi, S. Emoto, M. Kobayashi, T. Sugiura, and G. Vogel, Nucl. Fusion **51**, 063034 (2011).

[32] H. Saitoh, Z. Yoshida, J. Morikawa, Y. Yano, N. Kasaoka, W. Sakamoto, and T. Nogami, AIP Conf. Proc. **1521**, 63 (2013).

[33] M. Nishiura, Y. Kawazura, Z. Yoshida, N. Kenmochi, Y. Yano, H. Saitoh, M. Yamasaki, T. Mushiake, A. Kashyap, N. Takahashi, M. Nakatsuka, and A. Fukuyama, Nucl. Fusion **57**, 086038 (2017).

[34] E. Yatsuka, H. Kato, D. Sakata, J. Morikawa, Y. Ogawa, N. Yanagi, and T. Mito, Fusion Sci. Technol. **51**, 310 (2007).

[35] E. Yatsuka, K. Kinjo, J. Morikawa, and Y. Ogawa, Rev. Sci. Instrum. **80**, 023505 (2009).

[36] M. R. Stoneking, T. S. Pedersen, P. Helander, H. Chen, U. Hergenhahn, E. V. Stenson, G. Fiksel, J. Von Der Linden, H. Saitoh, C. M. Surko, J. R. Danielson, C. Hugenschmidt, J. Horn-Stanja, A. Mishchenko, D. Kennedy, A. Deller, A. Card, S. Nißl, M. Singer, M. Singer *et al.*, J. Plasma Phys. **86**, 155860601 (2020).

[37] J. Arons, Space Sci. Rev. **24**, 437 (1979).

[38] J. F. C. Wardle, D. C. Homan, R. Ojha, and D. H. Roberts, Nature (London) **395**, 457 (1998).

[39] T. Siegert, R. Diehl, J. Greiner, M. G. H. Krause, A. M. Beloborodov, M. C. Bel, F. Guglielmetti, J. Rodriguez, A. W. Strong, and X. Zhang, Nature (London) **531**, 341 (2016).

[40] A. Philippov, A. Timokhin, and A. Spitkovsky, Phys. Rev. Lett. **124**, 245101 (2020).

[41] V. Tsytovich and C. B. Wharton, Comments Plasma Phys. Control. Fusion **4**, 91 (1978).

[42] R. G. Greaves and C. M. Surko, Phys. Rev. Lett. **75**, 3846 (1995).

[43] S. J. Gilbert, D. H. E. Dubin, R. G. Greaves, and C. M. Surko, Phys. Plasmas. **8**, 4982 (2001).

[44] W. Oohara, D. Date, and R. Hatakeyama, Phys. Rev. Lett. **95**, 175003 (2005).

[45] T. S. Pedersen, J. R. Danielson, C. Hugenschmidt, G. Marx, X. Sarasola, F. Schauer, L. Schweikhard, C. M. Surko, and E. Winkler, New J. Phys. **14**, 035010 (2012).

[46] G. Sarri, K. Poder, J. M. Cole, W. Schumaker, A. Di Piazza, B. Reville, T. Dzelzainis, D. Doria, L. A. Gizzi, G. Grittani, S. Kar, C. H. Keitel, K. Krushelnick, S. Kuschel, S. P. D. Mangles, Z. Najmudin, N. Shukla, L. O. Silva, D. Symes, A. G. R. Thomas *et al.*, Nat. Commun. **6**, 6747 (2015).

[47] H. Higaki, C. Kaga, K. Fukushima, H. Okamoto, Y. Nagata, Y. Kanai, and Y. Yamazaki, New J. Phys. **19**, 023016 (2017).

[48] J. von der Linden, G. Fiksel, J. Peebles, M. R. Edwards, L. Willingale, A. Link, D. Mastrosimone, and H. Chen, Phys. Plasmas **28**, 092508 (2021).

[49] H. Chen and F. Fiuza, Phys. Plasmas **30**, 020601 (2023).

[50] P. Helander, Phys. Rev. Lett. **113**, 135003 (2014).

[51] E. V. Stenson, S. Nißl, U. Hergenhahn, J. Horn-Stanja, M. Singer, H. Saitoh, T. S. Pedersen, J. R. Danielson, M. R. Stoneking, M. Dickmann, and C. Hugenschmidt, Phys. Rev. Lett. **121**, 235005 (2018).

[52] B. E. O'Rourke, N. Oshima, A. Kinomura, T. Ohdaira, and R. Suzuki, Defect. Diffus. Forum. **331**, 75 (2012).

[53] C. M. Surko, M. Leventhal, and A. Passner, Phys. Rev. Lett. **62**, 901 (1989).

[54] H. Higaki, K. Michishio, K. Hashidate, A. Ishida, and N. Oshima, Appl. Phys. Express **13**, 066003 (2020).

[55] H. Higaki, K. Michishio, A. Ishida, and N. Oshima, Plasma Fusion Res. **18**, 1406023 (2023).

[56] R. G. Greaves and C. M. Surko, Phys. Rev. Lett. **85**, 1883 (2000).

[57] D. B. Cassidy, R. G. Greaves, V. E. Meligne, and A. P. Mills, Jr., Appl. Phys. Lett. **96**, 101502 (2010).

[58] J. R. Danielson, D. H. E. Dubin, R. G. Greaves, and C. M. Surko, Rev. Mod. Phys. **87**, 247 (2015).

[59] J. P. Marler and C. M. Surko, Phys. Rev. A **72**, 062702 (2005).

[60] A. R. Swann and D. G. Green, Phys. Rev. Lett. **130**, 033001 (2023).

[61] S. J. Gilbert, J. Sullivan, R. G. Greaves, and C. M. Surko, Nucl. Instrum. Meth. Phys. Res. Sec. B **171**, 81 (2000).

[62] S. Nißl, E. V. Stenson, U. Hergenhahn, J. Horn-Stanja, T. Sunn Pedersen, H. Saitoh, C. Hugenschmidt, M. Singer, M. R. Stoneking, and J. R. Danielson, Phys. Plasmas **27**, 052107 (2020).
[63] T. G. Northrop, Ann. Phys. **15**, 79 (1961).
[64] D. B. Cassidy, S. H. M. Deng, H. K. M. Tanaka, and A. P. Mills, Appl. Phys. Lett. **88**, 194105 (2006).
[65] D. B. Cassidy, Eur. Phys. J. D **72**, 53 (2018).
[66] J. von der Linden, S. Nißl, A. Deller, J. Horn-Stanja, J. R. Danielson, M. R. Stoneking, A. Card, T. Sunn Pedersen, and E. V. Stenson, J. Plasma Phys. **89**, 905890511 (2023).
[67] T. M. O'Neil, Phys. Scr. **T59**, 341 (1995).
[68] E. V. Stenson, J. Horn-Stanja, M. R. Stoneking, and T. S. Pedersen, J. Plasma Phys. **83**, 595830106 (2017).
[69] L. V. Jørgensen, M. Amoretti, G. Bonomi, P. D. Bowe, C. Canali, C. Carraro, C. L. Cesar, M. Charlton, M. Doser, A. Fontana, M. C. Fujiwara, R. Funakoshi, P. Genova, J. S. Hangst, R. S. Hayano, A. Kellerbauer, V. Lagomarsino, R. Landua, E. Lodi Rizzini, M. Macrì, and Y. Yamazaki (ATHENA Collaboration), Phys. Rev. Lett. **95**, 025002 (2005).
[70] D. W. Fitzakerley, M. C. George, E. A. Hessels, T. D. G. Skinner, C. H. Storry, M. Weel, G. Gabrielse, C. D. Hamley, N. Jones, K. Marable, E. Tardiff, D. Grzonka, W. Oelert, and M. Zielinski (ATRAP Collaboration), J. Phys. B **49**, 064001 (2016).
[71] A. Deller, C. W. Rogge, S. Desopo, E. V. Stenson, J. R. Danielson, M. R. Stoneking, C. Hugenschmidt, T. S. Pedersen, and C. M. Surko, J. Plasma Phys. **89**, 935890602 (2023).
[72] M. Singer, J. R. Danielson, S. König, T. S. Pedersen, L. Schweikhard, and E. V. Stenson, J. Plasma Phys. **89**, 935890501 (2023).
[73] K. S. Fine and C. F. Driscoll, Phys. Plasmas **5**, 601 (1998).
[74] J. P. Marler and M. R. Stoneking, Phys. Rev. Lett. **100**, 155001 (2008).
[75] P. Steinbrunner, T. M. O'Neil, M. R. Stoneking, and D. H. E. Dubin, J. Plasma Phys. **89**, 935890401 (2023).
[76] M. Singer, M. R. Stoneking, E. V. Stenson, S. Nißl, A. Deller, A. Card, J. Horn-Stanja, T. Sunn Pedersen, H. Saitoh, and C. Hugenschmidt, Phys. Plasmas **28**, 062506 (2021).